Journal of Environmental Chemical Engineering 9 (2021) 105275

Contents lists available at ScienceDirect

Journal of Environmental Chemical Engineering

journal homepage: www.elsevier.com/locate/jece

Adsorption of organic compounds from aqueous solution by pyridine-2-carboxaldehyde grafted MIL-101(Cr)-NH_2 metal-organic frameworks

Malcom Frimpong Dapaah [a,b], Baojian Liu [a,*], Liang Cheng [b]

[a] Zhejiang Provincial Key Laboratory for Biological and Chemical Processing Technologies of Farm Products, School of Biological and Chemical Engineering, Zhejiang University of Science and Technology, Hangzhou 310023, Zhejiang, China
[b] Biofuels Institute, School of the Environment and Safety Engineering, Jiangsu University, Zhenjiang 212013, China

ARTICLE INFO

Editor: Dr. Z. Wen

Keywords:
MIL-101-N-2-pyc
Kinetics
Isotherm studies
BPA
Regeneration

ABSTRACT

Metal-organic frameworks (MOFs) are of particular interest in the adsorption of organic pollutants. This study investigated the adsorption of aniline (ANI), furfural (FUR), and bisphenol A (BPA) in aqueous solution using MIL-101(Cr)-X (X = –H, $–NO_2$, $–NH_2$ and, –N-2-pyc), MIL-100(Cr, Fe), HKUST-1, and ZIF-8. For the first time, an imino-functionalized MOF was used to adsorb organic compounds in water. MOFs were characterized by XRD, N_2 adsorption-desorption, SEM, TEM, elemental analysis, and FTIR. MIL-101-N-2-pyc demonstrated the highest adsorption capacity of 460.8, 126.5, and 100.7 mg/g towards 500 mg/L BPA, ANI, and FUR respectively. The adsorption isotherms better suited the Langmuir model than the Freundlich model. Importantly, 98% of BPA (100 mg/L) was removed and the kinetic data correlated well with the pseudo-second-order model ($R^2 > 0.998$). Binary adsorption of FUR and acetic acid (AA) were determined for industrial relevance. MIL-101-N-2-pyc outperformed commercial activated carbon and the other MIL-101s with an impressive co-adsorption of 66.1 mg/g FUR and 62.5 mg/g AA. Overall, the adsorption mechanism was due to hydrogen bonding, π-π interaction, and electrostatic attraction. Moreover, MIL-101-N-2-pyc exhibited remarkable structural stability and less than 0.01 wt% Cr leached into water. The adsorbent regeneration was improved after 4 cycles in methanol.

1. Introduction

The current demand for more chemical-based commodities by the populace has no doubt caused an increase in industries all over the world. Despite the need for such intervention, the resulting higher pollutant discharge into the environment, be it land, air, or water, cannot be ruled out. A greater amount of industrial effluent contains compounds harmful and toxic to not only aquatic life, but humans as well. Some water pollutants that are largely endocrine disrupting compounds (EDCs) and pharmaceuticals and personal care products (PPCPs) can be categorized under contaminants of emerging concern [1]. EDCs adversely interfere with the regular functioning of hormones in humans. An example is bisphenol A (BPA), a compound for manufacturing epoxy resins and polycarbonate plastics [2]. Aniline (ANI) is known for its diverse applications in the pharmaceutical, plastic, dye, paint, and fertilizer industries [3]. It is noted to cause methemoglobinemia and cyanosis [4]. FUR, on the other hand, is useful in the pharmaceutical, plastic, and agrochemical industries [5]. In humans, it can adversely affect the liver and respiratory system [6]. In a bid to lessen concentrations of these pollutants, methods such as adsorption, photodecomposition, extraction, oxidation, bio-degradation, to mention a few, have been utilized. Among these techniques, adsorption has proven to be more versatile and cost-effective.

In our era of heightened technological advancements, the role of porous materials cannot be undermined as it finds vital use from industrial demands to domestic necessities. Remarkable porous materials in the research domain so far include zeolites, porous carbons, mesoporous silica, resin, metal-organic frameworks (MOFs), and so forth. MOFs stand out as a hybrid porous material made of metal ions and ligands joined together by coordination bonds. For the past decades, MOFs are utilized in areas such as gas storage, catalysis, drug delivery, separation as well as polluted air and water treatment [7–11]. Besides, several reviews have tackled MOFs related to liquid-phase adsorption of compounds in the aspects of performance [12], adsorption mechanism

* Corresponding author.
E-mail address: 107021@zust.edu.cn (B. Liu).

https://doi.org/10.1016/j.jece.2021.105275
Received 29 September 2020; Received in revised form 28 January 2021; Accepted 22 February 2021
Available online 24 February 2021

[13–15], and effect of functional groups [16]. On functionalized MOFs, Seo et al. [17] reported the use of urea-functionalized MIL-101(Cr) to adsorb 185 mg/g and 188 mg/g of dimetridazole (DMZ) and metronidazole (MNZ) respectively from water. The adsorption mechanism was attributed mainly to hydrogen bonding between pollutants and the amino/nitro-functional groups present.

So far, MOFs used for liquid-phase adsorption have been incorporated with popular functional groups such as $–NO_2$, $–SO_2H$, $–NH_2$, –OH, $–(OH)_3$, –COOH, $–(COOH)_2$, and –C=N–. To date, the incorporation of imine (–C=N–) groups into MOFs is limited to areas such as the adsorption of metals and water [18], metal and nitro-aromatics detection [19,20], oxidation [21], CO_2 capture, and catalysis [22]. To the best of our knowledge, there is no work on imine-functionalized MOFs being used for the liquid-phase adsorption of organic compounds.

Herein we report, for the first time, the application of a synthesized imino-pyridine MOF, MIL-101-N-2-pyc, for the removal of organic compounds from aqueous systems. This was conducted together with other MOFs; MIL-101(Cr) (pristine, $-NO_2$, and $-NH_2$), MIL-100(Cr, Fe), and commercial adsorbents (HKUST-1, ZIF-8, and AC (activated carbon)). The chemical structures of these pollutants (ANI, FUR, and BPA) are displayed in Fig. 1. MIL-101-N-2-pyc stood out with a significant sorption capacity towards these organic pollutants, especially BPA. Adsorption isotherm and kinetic studies were evaluated with related analysis models. Co-adsorption of acetic acid (AA) and FUR was demonstrated. Also, the adsorption mechanism in MIL-101-N-2-pyc was investigated. The work then concludes by analyzing the reusability of the imino-MOF.

2. Experimental section

2.1. Materials

All chemicals are commercially available and were used without further purification. Chromium (VI) oxide (CrO_3, 99.5%) was obtained from J&K Scientific Ltd. (Beijing, China). Nitroterephthalic acid (>98%) and 1,3,5-benzenetricarboxylic acid (>98%) were purchased from TCI (Shanghai, China). *N, N*-dimethylformamide (DMF) (>99.5%), $SnCl_2 2H_2O$ (>98%), acetonitrile (CH_3CN) (>99%), 2-pyridine carboxaldehyde (>98%), absolute ethanol (analytical reagent grade), hydrofluoric acid (HF) (>40%), nitric acid (HNO_3) (65−68%), and metallic iron powder (>98%) were purchased from Sinopharm Chemical Reagent Co., Ltd. (Shanghai, China). HPLC-grade methanol was supplied by Tedia Company Inc. (Fairfield, Ohio, U.S.A.). Hydrochloric acid (HCl, 37 wt%), acetic acid (>99.5%), activated carbon, and ANI (>99.5%) were gotten from Shanghai Lingfeng Chemical Reagent Co. Ltd. (Shanghai, China). $Cr(NO_3)_3 9H_2O$ (99%), ZIF-8, KHUST-1, and BPA were purchased from Sigma−Aldrich (Beijing, China). FUR (99%) was obtained from Aladdin Industrial Corporation (Shanghai, China). For this work, the hydrothermal approach was the synthesis route used for all MOFs.

2.2. Synthesis of MOFs

MIL-101(Cr): 2 g of $Cr(NO_3)_3 9H_2O$ (5 mmol), 0.82 g of terephthalic acid (5 mmol), and 0.25 g of 40 wt% HF solution (5 mmol) were mixed in a 45 mL Teflon-lined stainless steel autoclave containing 24 mL of water. The obtained precursor was placed in a stainless steel autoclave and heated at 220 °C for 8 h followed by cooling to room temperature. It was then centrifuged at 5000 revolutions per minute (rpm) for 10 min and also washed thrice per solvent in the order; deionized water, hot DMF (95 °C), and methanol. This was to remove any terephthalic acid present in the MOF. The final product was dried under vacuum [23].

MIL-101(Cr)-NO_2: 1.32 g of nitroterephthalic acid (6.25 mmol), 0.625 g of CrO_3 (6.25 mmol), and 0.9 g of 12 M hydrochloric acid (25 mmol) were mixed in a Teflon-lined stainless steel autoclave containing 25 mL water. The acidic mixture was heated at 180 °C for 6 days and then cooled to room temperature. The light green solids were centrifuged at 5000 rpm for 10 min followed by three times washing with deionized water, DMF, and methanol respectively. The nitro MOF was then dried under vacuum [24].

MIL-101(Cr)-NH_2: 1.5 g of MIL-101(Cr)-NO_2 and 24.45 g of $SnCl_2 2H_2O$ were mixed in 150 mL absolute ethanol. This was subjected to heating for 6 h at 70 °C with stirring. The green suspension formed, upon cooling to room temperature, was centrifuged at 5000 rpm for 10 min after which it was dispersed in 37 wt% HCl (150 mL) and shaken at 150 rpm for 9 h. It was then washed with deionized water and methanol (three times per solvent) after centrifugation. The green crystals were finally dried under vacuum [25].

MIL-101-N-2-pyc: 1.39 g of MIL-101-NH_2 and 2.25 g of pyridine-2-carboxaldehyde (21.0 mmol) were mixed in 15 mL of acetonitrile. The mixture was shaken at 150 rpm set to 40 °C for 12 h. The suspension was centrifuged at 5000 rpm for 10 min and then rinsed with 10 mL of fresh acetonitrile once daily for three days. It was then dried under vacuum at 80 °C before use [21].

MIL-100(Fe): metallic iron, Fe, was reacted with 1,3,5-benzenetricarboxylic acid, HF, HNO_3, and H_2O in the ratio 1: 0.66: 2.0: 1.2: 280. The mixture was kept at 150 °C in a Teflon-lined stainless steel autoclave for 6 days. The light-orange slurry was centrifuged at 5000 rpm for 10 min and rinsed with hot deionized water (80 °C) three times to decrease the residual amount of 1,3,5-benzenetricarboxylic acid. The product was then followed by drying at room temperature [26].

MIL-100(Cr): 1,3,5-benzenetricarboxylic acid, (5 mmol), chromium (VI) oxide (5 mmol), 5 mol/kg HF solution (1 mL) and 24 mL deionized water were placed in the 45 mL Teflon-lined stainless steel autoclave. It was stirred for some minutes at room temperature before subjection to 220 °C for 4 days. Upon cooling, the green slurry was centrifuged at 5000 rpm for 10 min and then rinsed three times each with hot water, DMF, and ethanol in a temperature-regulated shaker. The products were dried under vacuum [27].

2.3. Instruments

X-ray diffraction (XRD) patterns of synthesized MOFs were analyzed with an Ultima IV diffractometer (Rigaku, Tokyo, Japan) having a Cu Kα X-ray source ($\lambda = 1.54$ Å, scanning rate of 2° min^{-1} at 40 kV and 40 mA). Fourier transform infrared (FTIR) spectra were conducted using a Vertex 70 FTIR spectrometer (Bruker, Billerica, USA) by the KBr method in the range 4000–450 cm^{-1}. N_2 adsorption/desorption experiments were done at −196 °C using an ASAP 2460 surface area and porosimetry analyzer (Micromeritics, Georgia, USA). The

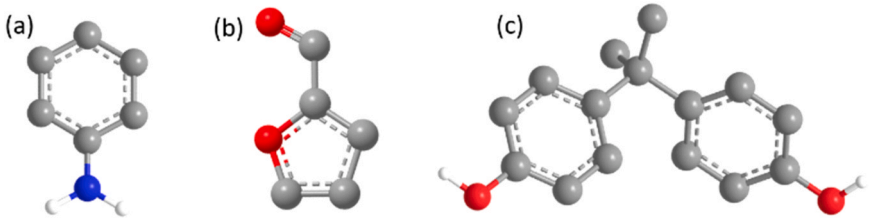

Fig. 1. Chemical structure of (a) ANI, (b) FUR, and (c) BPA.

Brunauer–Emmett–Teller (BET) method was used to calculate the specific surface areas of the crystals. Elemental constituents of materials were determined using a Vario MICRO cube analyzer (Elementar, Langenselbold, Germany). Surface morphology analysis was conducted using the SU-1510 scanning electron microscope (SEM) (Hitachi, Tokyo, Japan) and the Talos F200X transmission electron microscope (TEM) (Thermo Fischer Scientific, MA, USA). The surface elemental composition was assessed with an ESCALAB 250Xi X-ray photoelectron spectroscopy (XPS) (Thermo Fischer Scientific, MA, USA). Cr in water was determined using an ICP-OES700 analyzer (Agilent, CA, USA). Thermogravimetric analysis were carried out with a STA449F5 thermal analyzer (NETZSCH, Selb, Germany).

2.4. Batch adsorption

Before adsorption, the adsorbents were treated under vacuum for 12 h at 80 °C for MIL-101-N-2-pyc and 150 °C for the remaining materials respectively. This treatment was to eliminate all volatile impurities [23]. Different concentrations of adsorbates were prepared (50–500 mg/L) by dissolving ANI, FUR, and BPA in deionized water. The pH of the solutions was adjusted to 7. BPA solubility was enhanced by sonication with warming. About 10 mg of the adsorbents were mixed with 10 mL of varying solution concentrations in a set of vials (20 mL volume). The vials were sealed and placed in a THZ-92 shaker (Boxun, Shanghai, China) which was then set to 200 rpm for 24 h at 30 °C, sufficient to obtain adsorption equilibrium. After equilibrium, syringe filters (polytetrafluoroethylene, hydrophobic, 0.22 μm) were used to filter the solutions. The solute concentrations were analyzed using an Alliance e2695 high-performance liquid chromatography (HPLC) instrument furnished with a 2489 UV–Vis detector (Waters, MA, USA) and an ODS-C_{18} column (Waters Sunfire ™, 4.6 × 250 mm, inner diameter = 5 μm, MA, USA). The detection wavelengths and mobile phase (methanol: water), were set to 230 nm (50:50), 268 nm (20:80), and 215 nm (70:30) for ANI, FUR, and BPA respectively. An additional compound, acetic acid (AA) was also detected at 210 nm (3:97). The flow rate was kept at 1.0 mL min^{-1} whilst the column was maintained at 25 °C. The amount adsorbed was calculated based on the material balance:

$$q_e = \frac{V(C_o - C_e)}{m} \quad (1)$$

Where q_e is the amount adsorbed (mg/g) at equilibrium, V is the volume of the liquid solution (L), C_o and C_e are the initial and residue solute concentrations at equilibrium (mg/L), and m is the mass of adsorbent (g).

The kinetic studies involved exactly 10 mg of the top-performing adsorbent being placed into a series of vials (20 mL volume) after which 10 mL of 100 or 500 mg/L adsorbate solution was added. They were then shaken at 200 rpm at a temperature of 30 °C. A vial was taken out and filtered at preset time intervals for analysis using the Eq. (2);

$$q_t = \frac{V(C_o - C_t)}{m} \quad (2)$$

Where q_t is the amount adsorbed (mg/g) at time t, and C_t is the ANI, FUR, or BPA concentration at time t (mg/L).

To determine the removal efficiency, RE, of adsorbent towards ANI, FUR, and BPA, the following equation was used;

$$RE(\%) = \frac{C_0 - C_e}{C_0} \times 100 \quad (3)$$

The impact of pH during organic pollutant adsorption onto the MIL-MOF was evaluated. The solution pH of ANI, BPA, and FUR (500 mg/L) was varied from 2 to 10 by adding 0.1 M HCL and 0.1 M NaOH solutions. 10 mg of the adsorbent was mixed with 10 mL of the organic solutions at 30 °C for 12 h at 200 rpm.

For reusability studies, the spent MIL-101-N-2-pyc was centrifuged at 5000 rpm for 10 min and then desorbed with 10 mL of the eluents (ethanol, methanol, or acetonitrile) at 30 °C for 12 h in the shaker. This was followed by centrifugation and vacuum drying at 40 °C for 12 h. All experiments elaborated above were done in triplicates.

3. Results and discussion

3.1. Characterization

From Fig. 2(a), the unmodified materials; MIL-101(Cr), MIL-100(Fe), and MIL-100(Cr), showed higher N_2 uptake than the functionalized MOFs. This outcome is expected as the introduction of functional groups caused partial blockage of the MOF cages. The overall pattern was a sharp increase in adsorption at $P/P_o < 0.1$ then a gradual upsurge to $P/P_o < 0.25$, ending with a near-equilibrium before desorption. This signified type I physisorption isotherm and the microporous nature of prepared materials. Besides, the BET surface areas and pore volume of the MOFs are presented in Table 1. MIL-101(Cr) was significantly higher whilst the other frameworks were around half its value. MIL-101-N-2-pyc was found to have the least BET surface area due to its larger imino-pyridine structure attached. The parameters for MIL-100(Fe), and MIL-100(Cr) were observed to be lower for MIL-101(Cr), depicting higher porosity in MIL-101(Cr).

Deducing from elemental analysis (Table 1), the reduction of MIL-101-NO_2 to MIL-101-NH_2 was successful and marked by a 30.2% increase in H and 10.5% decrease in O. Condensation reaction between pyridine-2-carboxaldehyde and MIL-101-NH_2 led to a significant increase of 46.4%, 26.3%, 18.1%, and 13.5%, in N, C, H, and O respectively compared to MIL-101(Cr)-NH_2. The yield obtained was 34%. The corresponding elemental compositions of the other materials are also represented.

FTIR spectrum was used to characterize prepared MOFs considering the functional groups present (Fig. 2b). MIL-100(Fe) had a band at 1710 cm^{-1} which was ascribed to the stretching of C=O resulting from 1,3,5-benzenetricarboxylic acid remaining [28]. The 526 cm^{-1} peak in MIL-100(Cr) corresponded to Cr–O bond stretching [29]. MIL-101 was confirmed with 1397 cm^{-1} and 1625 cm^{-1} bands that represented symmetric (O–C–O) vibrations of dicarboxylate groups and the existence of adsorbed water molecules respectively [30,31]. Incorporation of $-NO_2$ into the MIL-101(Cr) structure was successful and this was evident as a stretching vibration was detected at 1540 cm^{-1} [25,32]. The stretching disappeared after MOF reduction with $SnCl_2$ and gave MIL-101(Cr)-NH_2. The band 1619 cm^{-1} corresponded to N-H bending whereas 1340 cm^{-1} referred to C–N stretching in the aromatic amine [33,34]. For MIL-101-N-2-pyc, the imine bond (C=N) resulted from moderate amino group conversion with pyridine-2-carboxaldehyde [21]. The C=N and unreacted aldehyde group (C=O) stretching were observed at 1656 cm^{-1} [35] and 1710 cm^{-1} [36] respectively. This confirmed the successful grafting of pyridine-2-carboxaldehyde.

XRD patterns of prepared MOFs were compared with simulated ones from the crystallographic data [37]. MIL-101(Cr), MIL-101(Cr)-NO_2, MIL-101(Cr)-NH_2, and MIL-101-N-2-pyc had their XRD patterns being isostructural with simulated MIL-101(Cr) indicating maintenance of the crystal structures after modification (Fig. 2c). That of MIL-100(Cr) and MIL-100(Fe) also agreed well with simulated MIL-100(Fe) (Fig. 2d).

From the SEM and TEM analysis (Fig. 3), surface morphologies of synthesized MIL-101(Cr) had smaller octahedral crystals. MIL-101(Cr)-NO_2 (Fig. 3b and h) and MIL-101(Cr)-NH_2 (Fig. 3c and i) showed mainly prismatic crystals which were earlier reported by Li et al. [38]. A similar structure was also observed for MIL-101-N-2-pyc (Fig. 3d and j). The presence of larger octahedral crystals [28] was seen in MIL-100(Fe) (Fig. 3e and k) whereas aggregation of spherical crystals appeared in MIL-100(Cr) (Fig. 3f and l). All structures confirmed the formation of MOFs as expected via the solvothermal process. Also, the molecular 3D space-filled packing orientation for these MOFs was visualized using their crystallographic data (Fig. S1).

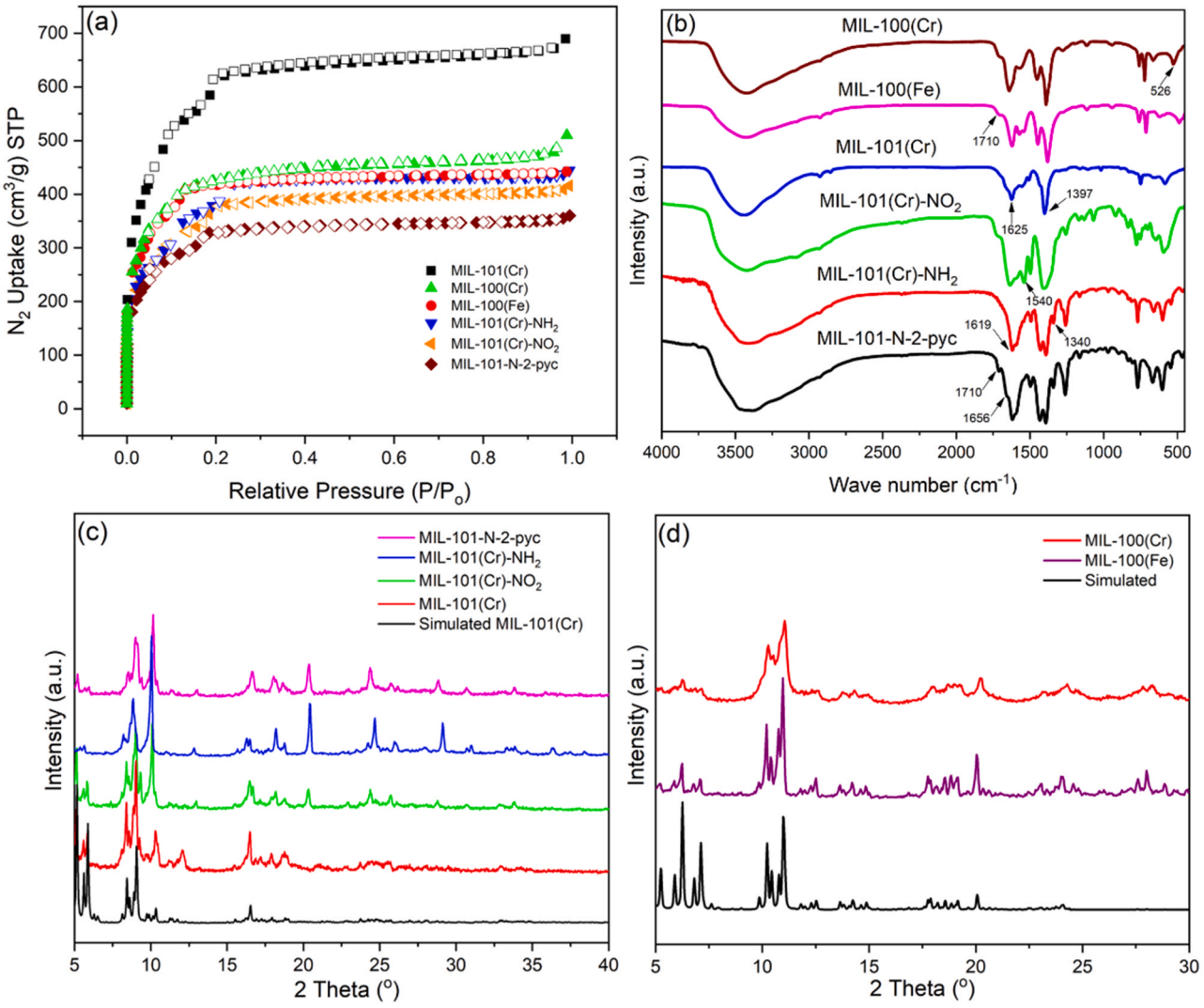

Fig. 2. (a) N_2 Isotherm linear plot, (b) FTIR spectra, (c,d) XRD profiles of MIL-101(Cr), MIL-100(Cr), MIL-100(Fe), MIL-101(Cr)-NH_2, MIL-101-N-2-pyc, and MIL-101(Cr)-NO_2.

Table 1
BET surface areas and total pore volume elemental constituents of prepared MOFs.

Material	S_{BET} (m^2/g)	V_{total}, (cm^3/g)	Elemental composition (wt%)			
			C	H	N	O
MIL-101(Cr)	2063	1.032	28.66	4.37	2.16	44.17
MIL-100(Fe)	1279	0.763	28.50	2.86	0.30	40.08
MIL-100(Cr)	1319	0.738	29.32	3.44	1.35	38.56
MIL-101(Cr)-NH_2	1443	0.670	26.60	4.31	3.17	37.30
MIL-101-N-2pyc	1037	0.544	33.60	5.09	4.64	42.35
MIL-101(Cr)-NO_2	1083	0.538	25.86	3.31	3.89	41.68

3.2. Adsorption isotherms

Batch-type adsorption experiments were carried out on synthesized MOFs and commercially available porous materials toward ANI, FUR, and BPA from 50 mg/L to 500 mg/L. As shown in Fig. 4(a), ANI adsorption capacity by the materials followed in this decreasing order; MIL-101-N-2-pyc > MIL-101(Cr)-NH_2 > MIL-101(Cr) > MIL-101(Cr)-NO_2 > AC > MIL-100(Cr) > ZIF-8 ≈ MIL-100(Fe) > HKUST-1. The dominance of the modified structures signaled improved interaction due to the specific functional groups present. The bulkier –imino-pyridine (12.8–126.5 mg/g) outperformed the –amino group (7.3–90.6 mg/g) regardless of its reduced BET surface area. The presence of imine constituents afforded more interaction sites for ANI in the partially blocked MIL-101(Cr) cages. Between MIL-101(Cr)-NH_2 and MIL-101(Cr)-NO_2, we earlier observed around 50% sorption increment in –NH_2 than –NO_2 towards N-compounds [39]. Better uptake here can be related to larger BET surface area, pore volume, and also improved sorbate-sorbent relationship in MIL-101(Cr)-NH_2 than MIL-101(Cr)-NO_2. Despite its functionality, MIL-101(Cr)-NO_2 material adsorbed lower than pristine MIL-101(Cr). This result indicated poor compatibility of the incorporated nitro group with ANI as well as the reduced surface area of the material. Analyzing the two different Cr structures, MIL-101(Cr) has a more expanded zeotype structure consisting of octahedral Cr(III) trimers linked by 1,4-benzenedicarboxylic acid, with two mesoporous cages of 29 and 34 Å diameter reachable through 12 and 16 Å microporous windows respectively [23]. MIL-100(Cr), on the other hand, is characterized by 6 and 9 Å micropores opening 24 and 27 Å mesoporous cages respectively [40]. These framework variances were confirmed by lower BET surface area and eventually lower adsorption of ANI in MIL-100(Cr). AC followed a quite different pathway that depicted quicker equilibrium whilst the MOFs were on the rise. ZIF-8, MIL-100(Fe), and

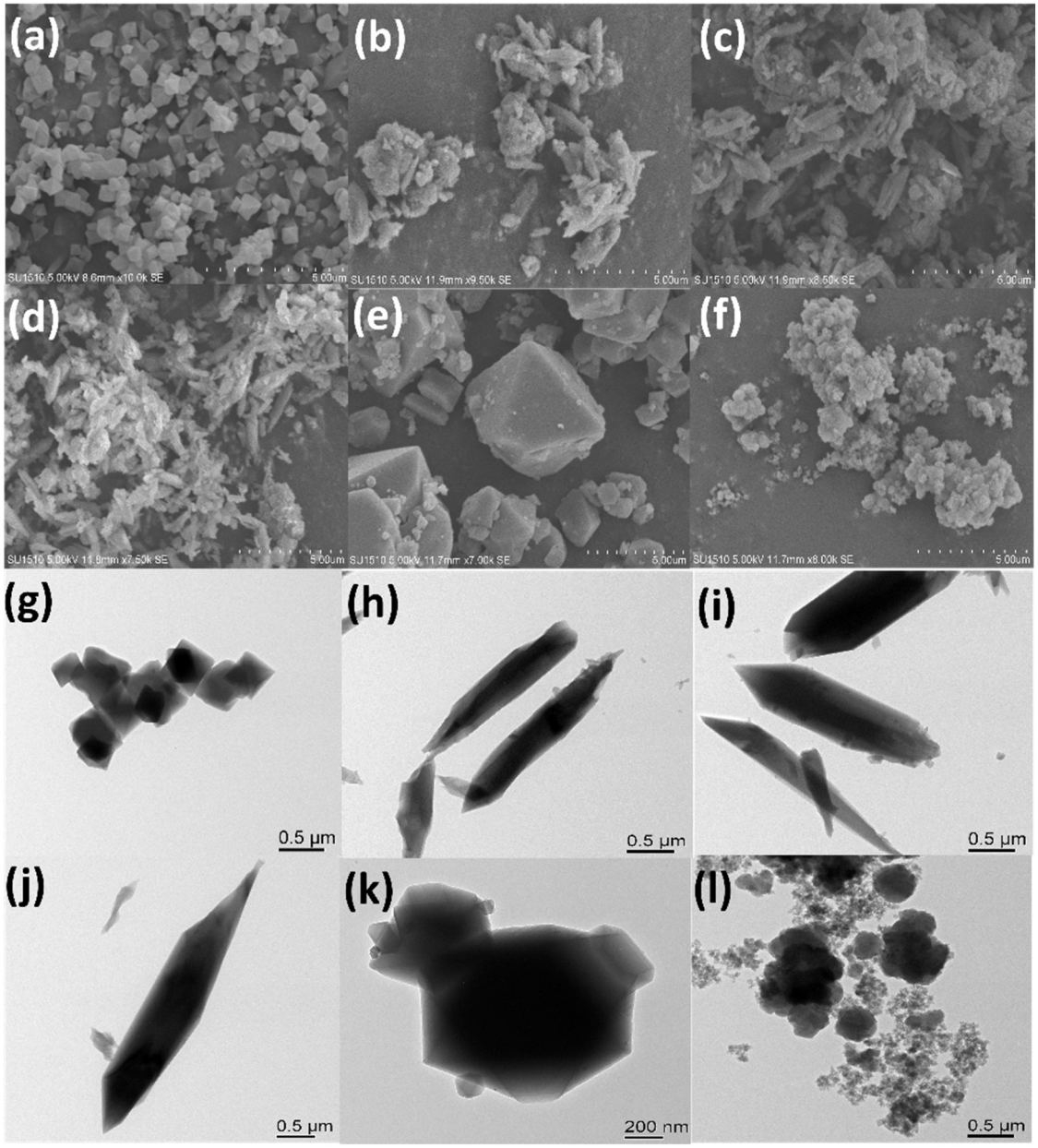

Fig. 3. SEM and TEM images for (a, g) MIL-101(Cr), (b, h) MIL-101(Cr)-NO_2, (c, i) MIL-101(Cr)-NH_2, (d, j) MIL-101-N-2-pyc, (e, k) MIL-100(Fe) and (f, l) MIL-100(Cr).

HKUST-1 had similarly low adsorptions. HKUST-1 adsorbed the least most probably due to its instability in water [41].

On FUR removal, a quite similar account was obtained which followed the sequence (Fig. 4b); MIL-101-N-2-pyc > MIL-101(Cr)-NH_2 > MIL-101(Cr) > MIL-101(Cr)-NO_2 > MIL-100(Cr) > AC > ZIF-8 > MIL-100(Fe) > HKUST-1. The adsorption pattern of MIIL-101(Cr)s towards ANI was also observed in FUR. This denoted common adsorbate characteristics (FUR kinetic diameter = 5.5 Å [42]; ANI kinetic diameter = 5.8 Å [43]). Further, MIL-100(Cr) this time performed quite better than AC for FUR removal. The likely reason can be attributed to the slightly lower kinetic diameter of FUR to ANI that caused easier penetration into MIL-100(Cr) cages. Such a minimum difference had little effect on AC. ZIF-8, MIL-100(Fe), and HKUST-1 adsorption capacities were more distinct though they had the same sequence with ANI.

Interestingly, a much different trend was observed for BPA removal (Fig. 4c). The adsorption isotherms for ANI and FUR appeared more linear than the BPA. This could be possibly due to the weaker adsorption affinities of the adsorbents for aniline and furfural compared to BPA. BPA adsorption isotherm followed the decreasing order; MIL-101-N-2-pyc > MIL-101(Cr)-NO_2 > AC > MIL-101(Cr)-NH_2 > MIL-101(Cr) > MIL-100(Fe) > MIL-100 (Cr) > ZIF-8 > HKUST-1. Beginning with MIL-101-N-2-pyc, its bulky imino functional group was expected to yield lower adsorption than MIL-101(Cr)-NO_2, however, this was not the case. This increment was ascribed to favorable interactions between the active sites in MIL-101-N-2-pyc and BPA. MIL-101(Cr)-NO_2 surprisingly yielded a greater adsorption capacity than MIL-101(Cr)-NH_2 notwithstanding its lower total pore volume and BET surface area. Such occurrence was related to stronger H bonding likely to exist between the more electronegative nitro group (O atom) and H centers in BPA than with the less electronegative amino group (N atom). Although MIL-101 (Cr)-NH_2 also showed reduced BET surface area compared to MIL-101 (Cr), its removal of BPA was higher. This can be expounded as the amino group in MIL-101(Cr)-NH_2 can induce hydrogen polar bonds

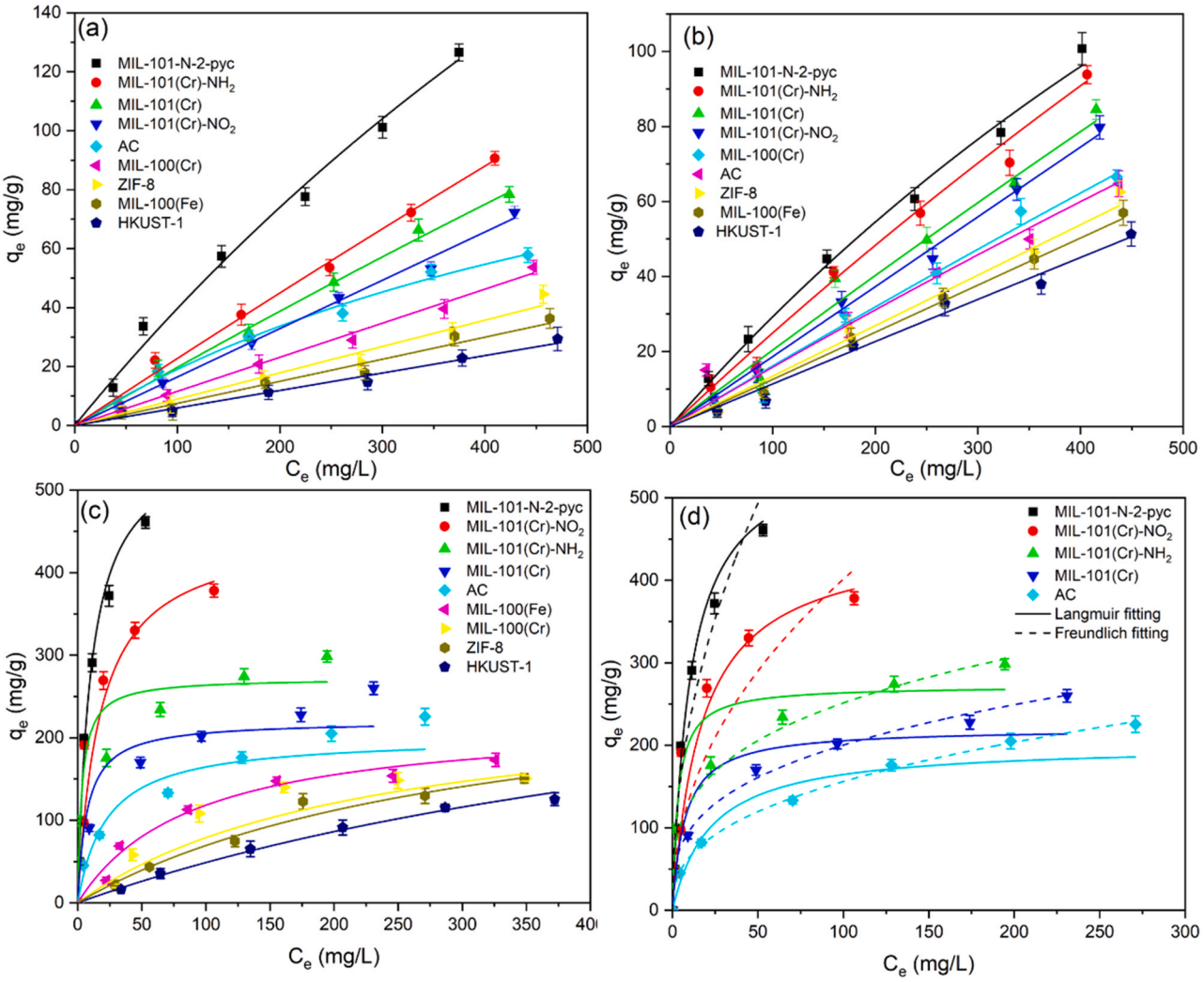

Fig. 4. Adsorption isotherms of (a) ANI, (b) FUR, (c) BPA onto MIL-101-N-2-pyc, MIL-101(Cr)-NH_2, MIL-101(Cr), MIL-101(Cr)-NO_2, AC, MIL-100(Cr), ZIF-8, MIL-100(Fe), and HKUST-1; (e) BPA onto MIL-101-N-2-pyc, MIL-101(Cr)-NH_2, MIL-101(Cr), MIL-101(Cr)-NO_2 and AC using Langmuir and Freundlich sorption isotherm models. Error bars represent the standard deviation of three replicates. (Adsorption conditions: temperature = 30 °C, agitation rate = 200 rpm, adsorbent mass = 0.01 g, pH = 7, and agitation time = 24 h).

between its N or H atoms and the H or O atoms of BPA respectively. The higher adsorption capacity in MIL-101(Cr) against AC pointed to more open sites resident in the Cr^{3+} material. Also, MIL-101(Cr) adsorbed more than MIL-100(Fe). This can be attributed to the BET surface area of MIL-101(Cr) being greater than MIL-100(Fe). Higher adsorption in MIL-100(Fe) than MIL-100(Cr) was due to the stronger binding energy of water with MIL-100(Cr) (−94.7 kJ/mol) than with MIL-100(Fe) (−75.5 kJ/mol) [44], which allowed easier interaction of MIL-100(Fe) with the adsorbate. For HKUST-1 and ZIF-8, Cu^{2+} and Zn^{2+} are intermediate Lewis acids, and hence their coordination with the BPA, a strong Lewis base was weak and this resulted in limited compound adsorption according to Pearson's hard-acid soft-base theory. On the other hand, Cr^{3+} metal sites in MIL-101s served as hard Lewis bases that resulted in improved interactions with hard BPA. The functionalized MIL-101s, parent MIL-101(Cr), and AC were selected for further analysis under isotherm models because of their higher adsorption capacities.

To analyze the adsorption isotherm of BPA on the synthesized MOFs and AC, Langmuir and Freundlich isotherm models were used (Fig. 4d). The Langmuir model is used to describe adsorption on a single layer. On the other hand, the Freundlich isotherm model is a multilayer adsorption concept involving heterogeneous surfaces that assumes that the bonding energy reduces exponentially with the occupied surface. The equations used for the correlations are as follows:

Langmuir model [45]:

$$q_e = \frac{q_m K_L C_e}{1 + K_L C_e} \tag{3}$$

Freundlich model [46]:

$$q_e = K_F C_e^{\frac{1}{n}} \tag{4}$$

where q_e is the amount of the desired compound adsorbed unto the adsorbent (mg/g), C_e is the equilibrium concentration (mg/L), K_L and K_F refer to Langmuir constant and Freundlich constant associated with adsorption capacity (L/mg) and ((mg/g) (L/mg) $^{1/n}$) respectively, whereas q_m is the theoretical maximum amount adsorbed to offer a complete monolayer (mg/g). n denotes adsorption intensity and when greater than 1, the adsorption of molecules occurs easily [47].

The isotherm points of MIL-101-N-2-pyc and MIL-101(Cr)-NO_2 were well correlated by the Langmuir isotherm model (R^2 of Langmuir isotherm = 0.905–0.973, R^2 of Freundlich isotherm = 0.873 – 0.930) (Table 2), which demonstrated the homogeneous nature of adsorbent surfaces in response to BPA adsorption. With the other materials, MIL-101(Cr), AC, and MIL-101(Cr)-NH_2 fitted better with the Freundlich isotherm model (R^2 of Langmuir isotherm = 0.948–0.976, R^2 of

Table 2
Isotherm parameters of BPA onto MIL-101(Cr) MOFs and AC (temperature = 30 °C, agitation rate = 200 rpm, adsorbent mass = 0.01 g, pH =7 and agitation time = 24 h).

Adsorbent	Langmuir			Freundlich		
	q_m (mg/g)	K_L (L/mg)	R^2	K_F [(mg/g) $(L/mg)^{1/n}$]	R^2	n
MIL-101-N-2-pyc	564.3	9.59×10^{-2}	0.973	75.7	0.930	2.087
MIL-101 (Cr)-NO_2	452.3	0.06×10^{-2}	0.905	46.4	0.873	2.135
MIL-101 (Cr)-NH_2	272.1	0.31×10^{-2}	0.948	66.4	0.976	3.461
MIL-101(Cr)	220.5	1.38×10^{-1}	0.953	46.9	0.999	3.172
AC	201.2	4.50×10^{-2}	0.976	26.7	0.999	2.608

Freundlich isotherm = 0.976 – 0.999). This denoted the existence of heterogeneous adsorption on these surfaces. Comparing its adsorption capacity with earlier reported adsorbents, the MIL-101-N-2-pyc material (q_m = 564.3 mg/g) was higher despite its smaller surface area (Table 3).

3.3. Adsorption kinetics

To ascertain how fast the adsorption process occurred on the top-performing MOF, kinetic studies of ANI, FUR, and BPA onto MIL-101-N-2-pyc was evaluated at 100 and 500 mg/L adsorbate concentrations. As observed in Fig. 5, two main stages were realized in the process of removing the organic compounds; (1) Stage I (contact time ≤ 3 h): It entailed a rapid upsurge in the uptake of organic compounds which depicted their physical adsorption onto the external surface of MIL-101-N-2-pyc. In (2) Stage II (contact time > 3 h), the pace of compound adsorption reduced significantly due to their seepage into internal surfaces of the microporous adsorbent till saturation was reached [48,49]. For both low and high concentrations, the beginning stage of adsorbate uptake onto the MOF was quite fast. The duration needed to approach adsorption equilibrium in ANI and FUR was within 6 h whereas, for BPA, 12 h was sufficient to reach saturation. Considering the kinetic diameters of FUR (5.5 Å), ANI (5.8 Å), and BPA (9.4 Å) [6], the bigger BPA molecules required more time than ANI or FUR molecules to diffuse into the functionalized MIL-101(Cr) (<12 Å) cages to be attached to the pore surfaces.

Removal efficiencies of FUR and ANI were quite close at 500 mg/L (R.E. of FUR = 23.3%; R.E. of ANI = 22.8%) but were slightly reduced at a lower initial concentration of 100 mg/L though still comparable (R.E. of FUR = 22.9%; R.E. of ANI = 23.4%). On the contrary, BPA removal efficiencies in both concentration cases were widely superior to ANI and FUR over four times in 100 mg/L (R.E. of BPA = 98.0%) and nearly four times in 500 mg/L (R.E. of BPA = 90.6%) respectively. This depicted favorable compatibility of MIL-101-N-2-pyc towards BPA based on variations in structural properties in BPA, ANI, and FUR.

Pseudo-first-order and pseudo-second-order models were used to simulate kinetic data obtained from aqueous adsorptions. The corresponding equations for pseudo-first-order [50] and pseudo-second-order [51] models are as follows respectively;

$$q_t = q_e(1 - e^{-k_1 t}) \quad (5)$$

$$q_t = \frac{t q_e^2 k_2}{t k_2 q_e + 1} \quad (6)$$

where q_e and q_t denote the amount of solute adsorbed (mg/g) at equilibrium and time t (h), respectively; k_1 and k_2 represent the rate constant of the pseudo-first-order adsorption (1/h) and pseudo-second-order adsorption (g/(mg.h)) respectively. Referring to Table 4, the correlation coefficients (R^2) at 100 and 500 mg/L initial concentrations demonstrated that the adsorption of BPA, ANI, FUR onto MIL-101-N-2-pyc fits better with pseudo-second-order model (R^2 = 0.976–0.999) than pseudo-first-order model (R^2 = 0.972–0.998). This signified chemical adsorption.

Table 3
Comparison of BET surface area and sorption capacities of BPA onto other adsorbents.

MOF	SA_{BET} (m^2/g)	q_m (mg/g)	Ref.
PCN-222	1914	487.69	[62]
PP-g-DMAEMA/PM composite fiber	193	327.8	[71]
Hard templated mesoporous carbon	1420	474	[72]
MIL-101(Cr)	3711	252.5	[63]
BMDC-12h	1449	714	[73]
Graphene	21	94.1	[74]
MSN-CTAB	131	155.8	[75]
pH Mesoporous silica	750	351	[76]
Al-ICR-6	1362	326	[77]
MIL-101-N-2-pyc	1037	564.3	This work

3.4. TGA-DSC analysis

To ascertain the stability of the prepared material, the thermal properties of MIL-101-N-2-pyc before and after BPA adsorption were examined using TGA-DSC analysis. From Fig. 6, two significant steps were observed, thus, 30–200 °C depicted the loss of water molecules whereas above 200 °C reflected the decomposition of the framework. Weight losses of 24% and 6% accompanied the first step for the fresh and used materials respectively. The reduced weight loss in the used material is likely due to the removal of the lesser water which was adsorbed because of existing BPA molecules in the framework [52]. Hence, a lower amount of energy was used to eliminate water molecules as shown by the reduced endothermic peak centered at 79 °C in the DSC profile. Generally, both materials showed similar decomposition patterns in DSC exothermic peaks and TG curves above 200 °C and 390 °C respectively. Therefore, the MIL-101-N-2-pyc adsorbent exhibited good thermal stability. Also, ICP-AES indicated that less than 0.01 wt% of Cr in MIL-101-N-2-pyc leached into the water.

3.5. XRD analysis

Inferring from the XRD patterns, MIL-101-N-2-pyc maintained its characteristic peaks after been treated with BPA (Fig. 7a). However, the intensity of the peaks reduced after BPA was present. This showed the stability of the MOF structure after adsorption.

3.6. FTIR analysis

The adsorption mechanism was confirmed by an analytical procedure. The FTIR spectrum of the MIL-101-N-2-pyc before and after BPA adsorption was assessed (Fig. 7b). A new band emerged at 2965 cm^{-1} which corresponded to CH stretching due to adsorbed BPA [53]. The peak increase and shift from 1501 cm^{-1} to 1512 cm^{-1} represented the vibration of aromatic C=C due to π-π interaction between benzene rings in MIL-101-N-2-pyc and BPA [54]. Also, the reduction of the peaks and upshift at 1656 cm^{-1} and 1710 cm^{-1} indicated the interaction of imine with BPA by hydrogen bonding.

3.7. XPS analysis

As shown in Fig. 8(a), the XPS spectrum of MIL-101-N-2-pyc consisted mainly of Cr, O, N, and C elements. Analysis of N 1s (Fig. 8b) offered three peaks at 398.8 eV, 399.7 eV, and 400.4 eV which were associated with pyridinic-N [55], amino groups [56], and imine groups [57] respectively. After BPA adsorption, N 1s experienced an upshift from 399.2 eV to 399.7 eV. This indicated the adsorption of BPA onto MIL-101-N-2-pyc was mainly influenced by N atoms. The resolved peaks at 399.7 eV and 400.4 eV increased from 27.6% and 34.6% to 40.6%

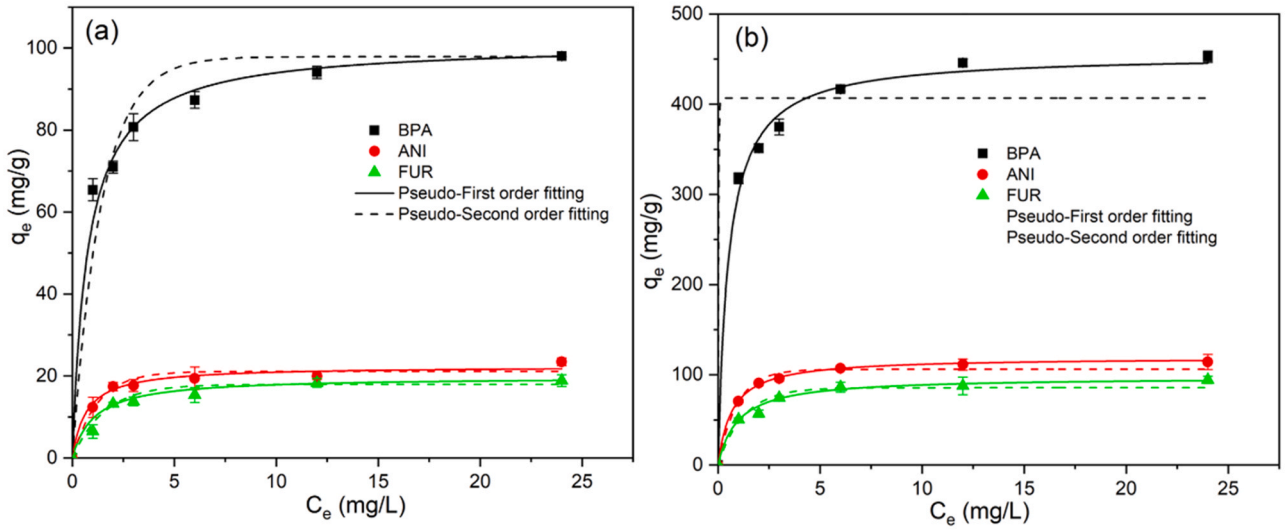

Fig. 5. Adsorption kinetics of ANI, FUR and BPA unto MIL-101-N-2-pyc at initial concentrations of (a) 100 mg/L and (b) 500 mg/L at 30 °C, pH = 7. Error bars represent the standard deviation of three replicates (V = 10 mL; m = 0.010 g; agitation rate = 200 rpm).

Table 4
Kinetic parameters for adsorption of BPA, ANI and FUR onto MIL-101-N-2-pyc (temperature = 30 °C, agitation rate = 200 rpm, pH = 7, and adsorbent mass = 0.01 g).

Adsorbate	C_o (mg/L)	$q_{e.exp}$ (mg/g)	Pseudo-first order model			Pseudo-second order model		
			$q_{e.cal}$ (mg/g)	k_1 (1/h)	R^2	$q_{e.cal}$ (mg/g)	k_2 (g/ (mg.h))	R^2
BPA	100	99.4	97.9	0.71	0.993	101.1	1.30×10^{-2}	0.999
	500	452.7	406.7	4.21	0.988	455.1	0.43×10^{-2}	0.999
ANI	100	23.4	21.1	0.82	0.972	22.4	1.30×10^{-2}	0.982
	500	114.3	106.1	1.07	0.998	119.3	1.23×10^{-2}	0.999
FUR	100	18.8	18.0	0.64	0.974	19.8	4.75×10^{-2}	0.976
	500	94.3	85.7	0.80	0.990	97.4	1.06×10^{-2}	0.997

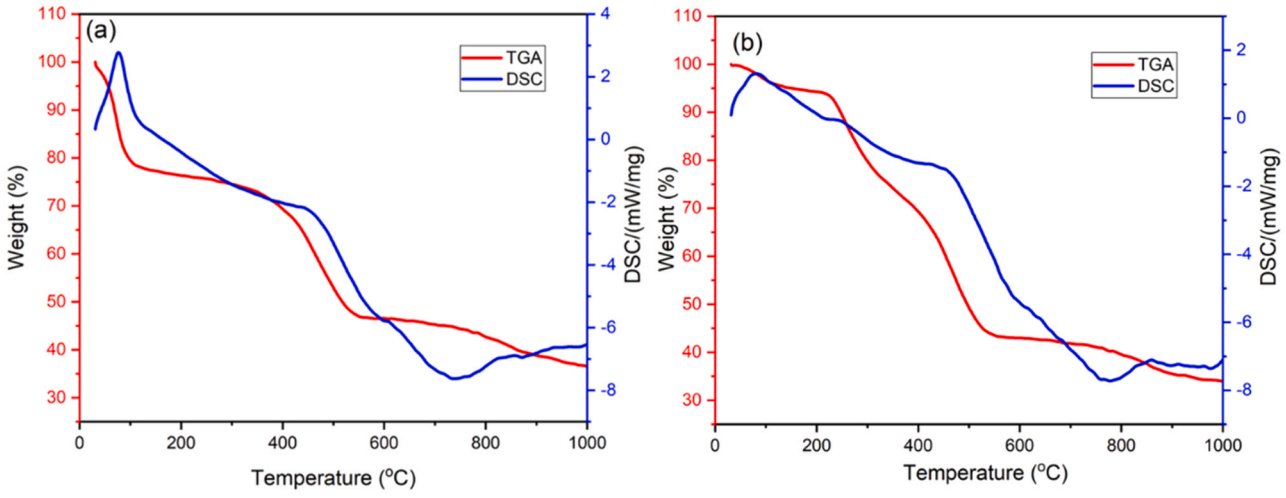

Fig. 6. TG-DSC analysis of MIL-101-N-2-pyc (a) before and (b) after BPA adsorption.

and 46.1% respectively. A significant decrease from 37.7% to 13.3% was observed at 398.8 eV. The upsurge denoted the interaction between BPA and the imino- and amino- groups through hydrogen bonding. The decrease in the pyridinic-N peak indicated its oxidation upon –OH attachment [58]. For the C 1s peak, four components represented as C–N, C = C, C=N and O–C=O were identified at 285 eV [59], 284.6 eV, 288 eV [57], and 288.52 eV [60] respectively (Fig. 8c). The C=C peak increased and this can be attributed to the proximity between the C=C rings in BPA and the pyridine in MIL-101-N-2-pyc. This confirmed π-π interaction earlier observed in FTIR. The C=N peak vastly reduced upon BPA adsorption as the characteristic bond was modified by –OH in BPA. Also, the C–N peak increased indicating a shift upon interaction. The increase in O–C=O peak indicated BPA interaction with the carboxylic acids inside the MOF structure.

3.8. Adsorption mechanisms

The underlying principle for the adsorption of pollutants onto the

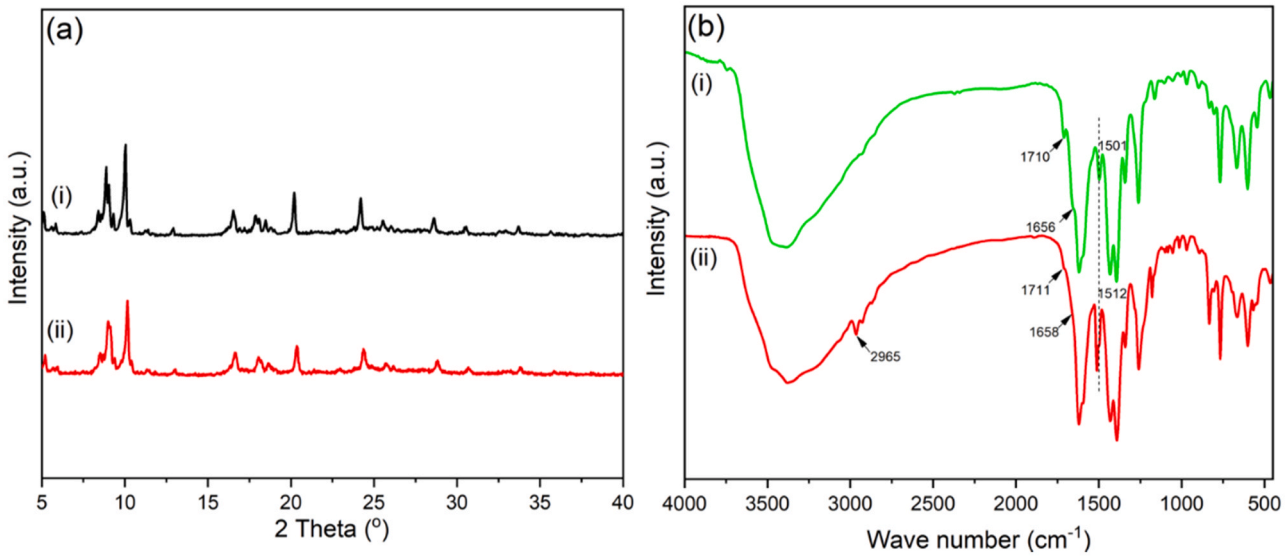

Fig. 7. XRD and FTIR spectra of MIL-101-N-2-pyc (a) before and (b) after BPA adsorption.

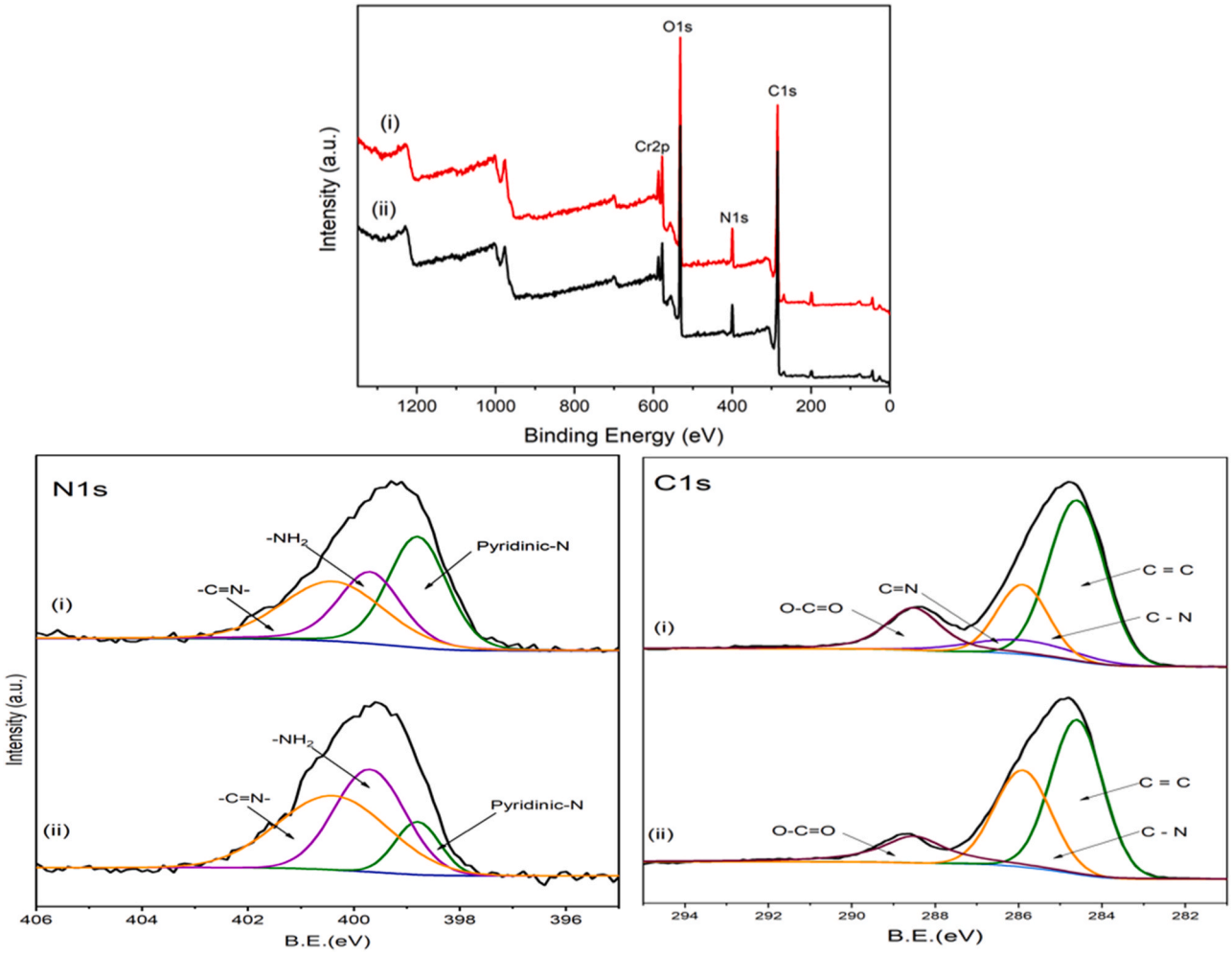

Fig. 8. (a) X-ray photoelectron spectrum of MIL-101-N-2-pyc, (b) N 1s, and (c) C 1s; (i) before and (ii) after BPA adsorption.

imino-functionalized MOF was explored considering possible interactions. From earlier works, the adsorption mechanisms of these pollutants involved electrostatic interactions, π-π, acid-base, pore structure, and H-bonding [61–64]. The pH of a solution in which adsorption occurs can affect the extent of ionization and surface charges especially when functional groups are involved [65]. With this basis, the

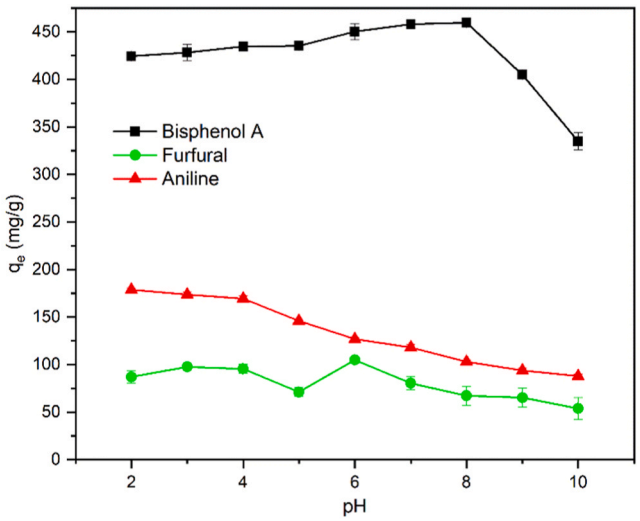

Fig. 9. Effect of pH variation from 2 to 10 on the adsorption of ANI, FUR, and BPA. Error bars represent the standard deviation of three replicates (adsorption conditions: temperature = 30 °C, agitation rate = 200 rpm, adsorbent mass = 0.01 g, and agitation time = 12 h).

influence of pH ranging from 2 to 10 was examined for the adsorption of pollutants. From Fig. 9, the adsorption of BPA was steady from a pH of 2 followed by a slight increment from pH 5 till 8, where the maximum capacity of 459.7 mg/g was reached. A distinct decrease was observed at pH > 8. This was ascribed to the pKa value of BPA which spans from 9.6 to 10.5 [66]. The hydroxyl groups in BPA deprotonated into phenolate ($HBPA^-$) and bisphenolate (BPA^{2-}) anions which were not favorably adsorbed by the MOF. BPA adsorption was improved when it existed in its molecular form [67]. Hence, electrostatic attraction of BPA is ruled out as solution pH was 7. In the case of ANI, the maximum adsorption of 178.7 mg/g occurred at a pH of 2. When the pH was below the pKa value of 4.6 [3], ANI was protonated into $C_6H_5NH^+$ which interacted better with the MOF surface. Upon pH increase, the adsorption reduced due to the existence of more molecular ANI than $C_6H_5NH^+$ [67]. Hence, electrostatic interaction occurred during ANI adsorption in the high pH region. For FUR, the maximum adsorption occurred at pH = 6. This was because FUR is stable at a natural pH_o of 6 and above or below this pH resulted in furoic acid or furfurylic alcohol production [68]. The variation of pH from 2 to 10 did not cause a significant adsorption difference. On hydrogen bonding, MIL-101-N-2-pyc has two nitrogen atoms (one in the ring and the other on the chain) which could attract the hydrogen atoms attached to electronegative nitrogen (ANI) and oxygen (BPA) atoms. For FUR, the absence of polar hydrogen atoms reduced the possibility to form a hydrogen bond with MIL-101-N-2-pyc. Besides, π-π interactions occurred between aromatic rings of FUR, BPA, and ANI and the pyridine ring resident in the MOF. The extent of adsorption in MIL-101-N-2-pyc towards ANI, FUR, and BPA varied amidst hydrogen bonding and π-π interactions. Superior sorption of BPA than ANI and FUR was due to the two benzene rings offering more sites for π-π interaction as against the single rings in ANI and FUR. Also, per the chemical structure, BPA has two hydrogen atoms attached to oxygen making them more polar than those attached to nitrogen in ANI. Overall, π-π interactions, electrostatic attraction and hydrogen bonding aided the adsorption of the organic pollutants.

3.9. Binary adsorption

In the effluent of FUR plants, the presence of FUR and AA are environmentally harmful as they pose threat to aquatic life [69]. Therefore

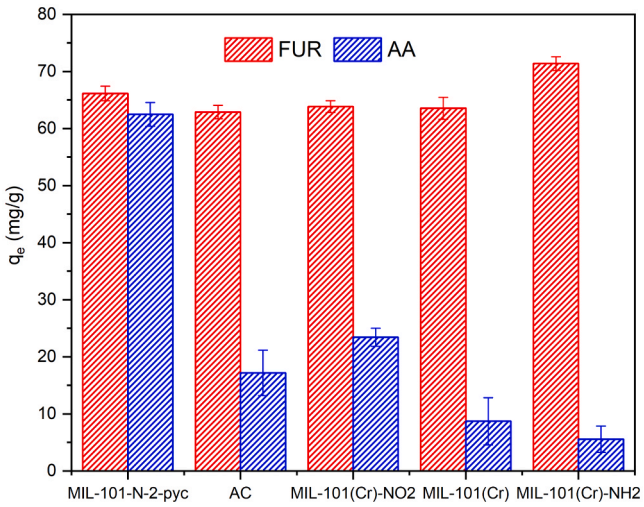

Fig. 10. Binary adsorption of FUR and AA onto MOFs and AC at 30 °C. Error bars represent the standard deviation of three replicates (adsorbent mass = 0.025 g, agitation rate = 200 rpm, and pH = 6).

to examine the adsorption in real-life systems, a ternary (FUR + water + AA) mixture was examined for binary adsorption of these pollutants. The ratio (w/w) of solutes in the mixture was 50:50 at a pH of 6. From Fig. 10, MIL-101-N-2-pyc displayed a strong affinity for both FUR (66.1 mg/g) and AA (62.5 mg/g) as compared to the other materials. The high co-adsorption might be due to more available adsorption sites that resulted in two probabilities; (1) formation of hydrogen bonds between MIL-101-N-2-pyc and polar hydrogen atoms in acetic acid and (2) π-π interactions between aromatic FUR and the imino-pyridine MOF. This makes it a choice material for removing pollutants in multicomponent (binary) mixtures. On the other hand, the remaining materials were more selective toward FUR than AA and they followed the sequence; MIL-101(Cr)-NH_2 > MIL-101(Cr) > AC > MIL-101(Cr)-NO_2. Therefore, in cases where FUR is much preferred to AA, the amino-MOF (FUR = 71.4 mg/g and AA = 5.6 mg/g) is the choice adsorbent. Although AA formed hydrogen bonds with MIL-101(Cr)-NH_2, its poor interaction was because of a stronger hydrogen bond with water molecules [70] than with the amino group. FUR was hence able to favorably hydrogen bond with MIL-101(Cr)-NH_2.

3.10. Reusability

The reusability of an adsorbent makes it more cost-efficient and beneficial for practical application. Three eluents (ethanol, methanol, and acetonitrile) were used to optimize the reusability of the adsorbent. The regenerated MOFs were used for BPA removal up to four times and the amounts adsorbed per cycle were calculated. From Fig. 11, the overall adsorption capacity for 500 mg/L BPA was reduced to 423.6 mg/g, 408.3 mg/g, and 395.5 mg/g after four recycle times for methanol, ethanol, and acetonitrile respectively. Therefore, methanol enhanced the reusability of MIL-101-N-2-pyc.

4. Conclusion

In this study, the aqueous adsorptions of organic pollutants, thus BPA, FUR, and ANI onto MIL-101(Cr)-X (X = -H, -NO_2, -NH_2 and, -N-2-pyc), MIL-100(Cr, Fe), HKUST-1, and ZIF-8 were investigated. The prepared materials were characterized by XRD, FTIR, elemental analysis, SEM, TEM, and N_2 adsorption-desorption studies. MIL-101-N-2-pyc best adsorbed all compounds under study. This is the first time an imino-

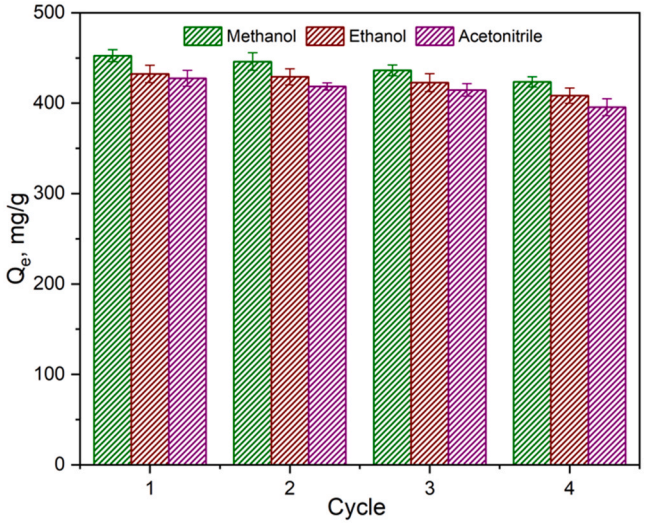

Fig. 11. (a) Adsorption capacities of BPA on the regenerated MIL-101-N-2-pyc up to four recycle times. Error bars represent the standard deviation of three replicates (adsorption conditions: temperature = 30 °C, agitation rate = 200 rpm, pH = 8, and agitation time = 12 h).

functionalized MOF is used to adsorb organic pollutants in aqueous systems. Besides, isotherm studies were better fitted by the Langmuir model and kinetic data were well correlated by the pseudo-second-order model. Additional, favorable co-adsorption of FUR and AA was achieved using the choice adsorbent. The plausible adsorption mechanism was attributed to hydrogen-bond, π-π interactions, and electrostatic attraction. Finally, MIL-101-N-2-pyc was easily regenerated using methanol for up to 4 cycles.

CRediT authorship contribution statement

Malcom Frimpong Dapaah: Data curation, Formal analysis, Investigation, Software, Visualization, Writing - original draft. **Baojian Liu**: Conceptualization, Funding acquisition, Supervision, Methodology, Validation, Resources, Project administration, Writing - review & editing. **Liang Cheng**: Funding acquisition, Writing - review & editing.

Declaration of Competing Interest

The authors declare no conflict of interest.

Acknowledgments

This work was supported by the National Natural Science Foundation of China (Grant no. 21576242). The authors are also grateful for the support from the program of Jiangsu Distinguished Professor and the Innovation/Entrepreneurship Program of Jiangsu Province.

Appendix A. Supporting information

Supplementary data associated with this article can be found in the online version at doi:10.1016/j.jece.2021.105275.

References

[1] Y. Yoon, J. Ryu, J. Oh, B.-G. Choi, S.A. Snyder, Occurrence of endocrine disrupting compounds, pharmaceuticals, and personal care products in the Han river (Seoul, South Korea), Sci. Total Environ. 408 (2010) 636–643, https://doi.org/10.1016/j.scitotenv.2009.10.049.

[2] G. Xiao, L. Fu, A. Li, Enhanced adsorption of bisphenol A from water by acetylaniline modified hyper-cross-linked polymeric adsorbent: effect of the cross-linked bridge, Chem. Eng. J. 191 (2012) 171–176, https://doi.org/10.1016/j.cej.2012.02.092.

[3] X. Li, X. Jin, N. Zhao, I. Angelidaki, Y. Zhang, Efficient treatment of aniline containing wastewater in bipolar membrane microbial electrolysis cell-fenton system, Water Res. 119 (2017) 67–72, https://doi.org/10.1016/j.watres.2017.04.047.

[4] D. Wilburn-Goo, L.M. Lloyd, When patients become cyanotic: acquired methemoglobinemia, J. Am. Dent. Assoc. 130 (1999) 826–831, https://doi.org/10.14219/jada.archive.1999.0306.

[5] A.S. Mamman, J. Lee, Y. Kim, I.T. Hwang, N. Park, Y.K. Hwang, J. Chang, J. Hwang, Furfural: hemicellulose/xylosederived biochemical, Biofuels Bioprod. Biorefin. Innov. Sustain. Econ. 2 (2008) 438–454, https://doi.org/10.1002/bbb.95.

[6] N.R. Reed, E.S.C. Kwok, Furfural, in: P. Wexler (Ed.), Encyclopedia of Toxicology, Third ed., Academic Press, Oxford, 2014, pp. 685–688, https://doi.org/10.1016/B978-0-12-386454-3.00147-0.

[7] Y. Peng, V. Krungleviciute, I. Eryazici, J.T. Hupp, O.K. Farha, T. Yildirim, Methane storage in metal-organic frameworks: current records, surprise findings, and challenges, J. Am. Chem. Soc. 135 (2013) 11887–11894, https://doi.org/10.1021/ja4045289.

[8] R.M. Abdelhameed, M. Abu-Elghait, M. El-Shahat, Hybrid three MOFs composites (ZIF-67@ZIF-8@MIL-125-NH2): enhancement the biological and visible-light photocatalytic activity, J. Environ. Chem. Eng. 8 (2020), 104107, https://doi.org/10.1016/j.jece.2020.104107.

[9] R.C. Huxford, J. Della Rocca, W. Lin, Metal–organic frameworks as potential drug carriers, Curr. Opin. Chem. Biol. 14 (2010) 262–268, https://doi.org/10.1016/j.cbpa.2009.12.012.

[10] F. Gholami, S. Zinadini, A.A. Zinatizadeh, Preparation of high performance CuBTC/PES ultrafiltration membrane for oily wastewater separation; a good strategy for advanced separation, J. Environ. Chem. Eng. 8 (2020), 104482, https://doi.org/10.1016/j.jece.2020.104482.

[11] Alamgir, K. Talha, B. Wang, J.-H. Liu, R. Ullah, F. Feng, J. Yu, S. Chen, J.-R. Li, Effective adsorption of metronidazole antibiotic from water with a stable Zr(IV)-MOFs: insights from DFT, kinetics and thermodynamics studies, J. Environ. Chem. Eng. 8 (2020), 103642, https://doi.org/10.1016/j.jece.2019.103642.

[12] S. Dhaka, R. Kumar, A. Deep, M.B. Kurade, S.W. Ji, B.H. Jeon, Metal–organic frameworks (MOFs) for the removal of emerging contaminants from aquatic environments, Coord. Chem. Rev. 380 (2019) 330–352, https://doi.org/10.1016/j.ccr.2018.10.003.

[13] Z. Hasan, S.H. Jhung, Removal of hazardous organics from water using metal-organic frameworks (MOFs): plausible mechanisms for selective adsorptions, J. Hazard. Mater. 283 (2015) 329–339, https://doi.org/10.1016/j.jhazmat.2014.09.046.

[14] L. Joseph, B.M. Jun, M. Jang, C.M. Park, J.C. Muñoz-Senmache, A.J. Hernández-Maldonado, A. Heyden, M. Yu, Y. Yoon, Removal of contaminants of emerging concern by metal-organic framework nanoadsorbents: a review, Chem. Eng. J. 369 (2019) 928–946, https://doi.org/10.1016/j.cej.2019.03.173.

[15] I. Ahmed, S.H. Jhung, Applications of metal-organic frameworks in adsorption/separation processes via hydrogen bonding interactions, Chem. Eng. J. 310 (2017) 197–215, https://doi.org/10.1016/j.cej.2016.10.115.

[16] D.K. Yoo, B.N. Bhadra, S.H. Jhung, Adsorptive removal of hazardous organics from water and fuel with functionalized metal-organic frameworks: contribution of functional groups, J. Hazard. Mater. 403 (2021), 123655, https://doi.org/10.1016/j.jhazmat.2020.123655.

[17] P.W. Seo, N.A. Khan, S.H. Jhung, Removal of nitroimidazole antibiotics from water by adsorption over metal–organic frameworks modified with urea or melamine, Chem. Eng. J. 315 (2017) 92–100, https://doi.org/10.1016/j.cej.2017.01.021.

[18] H. Zhu, J. Yuan, X. Tan, W. Zhang, M. Fang, X. Wang, Efficient removal of Pb^{2+} by Tb-MOFs: identifying the adsorption mechanism through experimental and theoretical investigations, Environ. Sci. Nano 6 (2019) 261–272, https://doi.org/10.1039/C8EN01066H.

[19] J. Wang, T. Xia, X. Zhang, Q. Zhang, Y. Cui, Y. Yang, G. Qian, A turn-on fluorescent probe for Cd^{2+} detection in aqueous environments based on an imine functionalized nanoscale metal–organic framework, RSC Adv. 7 (2017) 54892–54897, https://doi.org/10.1039/C7RA11162B.

[20] S. Tarasi, A. Azhdari Tehrani, A. Morsali, P. Retailleau, Fabrication of amine and imine-functionalized isoreticular pillared-layer metal–organic frameworks for the highly selective detection of nitro-aromatics, New J. Chem. 42 (2018) 14772–14778, https://doi.org/10.1039/C8NJ02407C.

[21] H. Liu, D. Ramella, P. Yu, Y. Luan, A novel modified MIL-101-NH2 ligand for CuI-catalyzed and air promoted oxidation of secondary alcohols, RSC Adv. 7 (2017) 22353–22359, https://doi.org/10.1039/C7RA00296C.

[22] U.S.F. Arrozi, V. Bon, S. Krause, T. Lübken, M.S. Weiss, I. Senkovska, S. Kaskel, In situ imine-based linker formation for the synthesis of zirconium MOFs: a route to CO_2 capture materials and ethylene oligomerization catalysts, Inorg. Chem. 59 (2020) 350–359, https://doi.org/10.1021/acs.inorgchem.9b02517.

[23] S. Bhattacharjee, C. Chen, W.-S. Ahn, Chromium terephthalate metal–organic framework MIL-101: synthesis, functionalization, and applications for adsorption and catalysis, RSC Adv. 4 (2014) 52500–52525, https://doi.org/10.1039/C4RA11259H.

[24] G. Akiyama, R. Matsuda, H. Sato, A. Hori, M. Takata, S. Kitagawa, Effect of functional groups in MIL-101 on water sorption behavior, Microporous Mesoporous Mater. 157 (2012) 89–93, https://doi.org/10.1016/j.micromeso.2012.01.015.

[25] S. Bernt, V. Guillerm, C. Serre, N. Stock, Direct covalent post-synthetic chemical modification of Cr-MIL-101 using nitrating acid, Chem. Commun. 47 (2011) 2838, https://doi.org/10.1039/c0cc04526h.

[26] P. Horcajada, S. Surblé, C. Serre, D.-Y. Hong, Y.-K. Seo, J.-S. Chang, J.-M. Grenèche, I. Margiolaki, G. Férey, Synthesis and catalytic properties of MIL-100 (Fe), an iron(iii) carboxylate with large pores, Chem. Commun. (2007) 2820–2822, https://doi.org/10.1039/B704325B.

[27] G. Førey, C. Serre, C. Mellot-, J. Dutour, A hybrid solid with giant pores prepared by a combination of targeted chemistry, Simul. Powder Diffr. (2004) 6296–6301, https://doi.org/10.1002/anie.200460592.

[28] J. Shi, S. Hei, H. Liu, Y. Fu, F. Zhang, Y. Zhong, W. Zhu, Synthesis of MIL-100(Fe) at low temperature and atmospheric pressure, J. Chem. 2013 (2013) 1–4, https://doi.org/10.1155/2013/792827.

[29] M. Songolzadeh, M. Soleimani, M.T. Ravanchi, Evaluation of metal type in MIL-100 structure to synthesize a selective adsorbent for the basic N-compounds removal from liquid fuels, Microporous Mesoporous Mater. 274 (2019) 54–60, https://doi.org/10.1016/j.micromeso.2018.07.032.

[30] S.H. Jhung, J.H. Lee, J.W. Yoon, C. Serre, G. Férey, J.S. Chang, Microwave synthesis of chromium terephthalate MIL-101 and its benzene sorption ability, Adv. Mater. 19 (2007) 121–124, https://doi.org/10.1002/adma.200601604.

[31] Q. Liu, L. Ning, S. Zheng, M. Tao, Y. Shi, Y. He, Adsorption of carbon dioxide by MIL-101(Cr): regeneration conditions and influence of flue gas contaminants, Sci. Rep. 3 (2013) 2916, https://doi.org/10.1038/srep02916.

[32] X. Li, Y. Mao, K. Leng, G. Ye, Y. Sun, W. Xu, Synthesis of amino-functionalized MIL-101(Cr) with large surface area, Mater. Lett. 197 (2017) 192–195, https://doi.org/10.1016/j.matlet.2017.03.034.

[33] X. Huang, J. Lu, W. Wang, X. Wei, J. Ding, Experimental and computational investigation of CO_2 capture on amine grafted metal-organic framework NH2-MIL-101, Appl. Surf. Sci. 371 (2016) 307–313, https://doi.org/10.1016/j.apsusc.2016.02.154.

[34] Y. Lin, C. Kong, L. Chen, Direct synthesis of amine-functionalized MIL-101(Cr) nanoparticles and application for CO_2 capture, RSC Adv. 2 (2012) 6417–6419, https://doi.org/10.1039/C2RA20641B.

[35] L. Feng, K.-Y. Wang, X.-L. Lv, J.A. Powell, T.-H. Yan, J. Willman, H.-C. Zhou, Imprinted apportionment of functional groups in multivariate metal–organic frameworks, J. Am. Chem. Soc. 141 (2019) 14524–14529, https://doi.org/10.1021/jacs.9b06917.

[36] Y. Qin, B. Wang, J. Li, X. Wu, L. Chen, Cobalt imine–pyridine–carbonyl complex functionalized metal–organic frameworks as catalysts for alkene epoxidation, Transit. Met. Chem. (2019) 1–8, https://doi.org/10.1007/s11243-019-00319-1.

[37] S. Gražulis, A. Daškevič, A. Merkys, D. Chateigner, L. Lutterotti, M. Quiros, N. R. Serebryanaya, P. Moeck, R.T. Downs, A. Le Bail, Crystallography open database (COD): an open-access collection of crystal structures and platform for world-wide collaboration, Nucleic Acids Res. 40 (2012) D420–D427, https://doi.org/10.1093/nar/gkr900.

[38] C.-R. Lim, S. Lin, Y.-S. Yun, Highly efficient and acid-resistant metal-organic frameworks of MIL-101(Cr)-NH2 for Pd(II) and Pt(IV) recovery from acidic solutions: adsorption experiments, spectroscopic analyses, and theoretical computations, J. Hazard. Mater. 387 (2020), 121689, https://doi.org/10.1016/j.jhazmat.2019.121689.

[39] B. Liu, Y. Peng, Q. Chen, Adsorption of N/S-heteroaromatic compounds from fuels by functionalized MIL-101(Cr) metal–organic frameworks: the impact of surface functional groups, Energy Fuels 30 (2016) 5593–5600, https://doi.org/10.1021/acs.energyfuels.6b00858.

[40] O.A. Kholdeeva, I.Y. Skobelev, I.D. Ivanchikova, K.A. Kovalenko, V.P. Fedin, A. B. Sorokin, Hydrocarbon oxidation over Fe- and Cr-containing metal-organic frameworks MIL-100 and MIL-101–a comparative study, Catal. Today 238 (2014) 54–61, https://doi.org/10.1016/j.cattod.2014.01.010.

[41] Y.-H. Shih, Y.-C. Kuo, S. Lirio, K.-Y. Wang, C.-H. Lin, H.-Y. Huang, A simple approach to enhance the water stability of a metal-organic framework, Chem. – A Eur. J. 23 (2017) 42–46, https://doi.org/10.1002/chem.201603647.

[42] K. Wang, J. Zhang, B.H. Shanks, R.C. Brown, Catalytic conversion of carbohydrate-derived oxygenates over HZSM-5 in a tandem micro-reactor system, Green Chem. 17 (2015) 557–564, https://doi.org/10.1039/C4GC01784F.

[43] L. Xu, Q. Yao, Y. Zhang, Y. Fu, Integrated production of aromatic amines and N-doped carbon from lignin via ex situ catalytic fast pyrolysis in the presence of ammonia over zeolites, ACS Sustain. Chem. Eng. 5 (2017) 2960–2969, https://doi.org/10.1021/acssuschemeng.6b02542.

[44] M. Tong, D. Liu, Q. Yang, S. Devautour-Vinot, G. Maurin, C. Zhong, Influence of framework metal ions on the dye capture behavior of MIL-100 (Fe, Cr) MOF type solids, J. Mater. Chem. A 1 (2013) 8534–8537, https://doi.org/10.1039/C3TA11807J.

[45] I. Langmuir, The adsorption of gases on plane surfaces of glass, mica and platinum, J. Am. Chem. Soc. 40 (1918) 1361–1403, https://doi.org/10.1021/ja02242a004.

[46] R. Van Bladel, A. Moreale, Adsorption of herbicide-derived p-chloroaniline residues in soils: a predictive equation, J. Soil Sci. 28 (1977) 93–102, https://doi.org/10.1111/j.1365-2389.1977.tb02298.x.

[47] R. Kecili, C.M. Hussain, Mechanism of adsorption on nanomaterials, in: C. M. Hussain (Ed.), Nanomaterials in Chromatography, 1st ed., Elsevier, 2018, pp. 89–115.

[48] R. Han, J. Zhang, P. Han, Y. Wang, Z. Zhao, M. Tang, Study of equilibrium, kinetic and thermodynamic parameters about methylene blue adsorption onto natural zeolite, Chem. Eng. J. 145 (2009) 496–504, https://doi.org/10.1016/j.cej.2008.05.003.

[49] S. Wang, E. Ariyanto, Competitive adsorption of malachite green and Pb ions on natural zeolite, J. Colloid Interface Sci. 314 (2007) 25–31, https://doi.org/10.1016/j.jcis.2007.05.032.

[50] H. Yuh-Shan, Citation review of Lagergren kinetic rate equation on adsorption reactions, Scientometrics 59 (2004) 171–177, https://doi.org/10.1023/B:SCIE.0000013305.99473.cf.

[51] Y.S. Ho, G. Mckay, Pseudo-Second Order Model Sorpt. Process., 34, 1999, pp. 451–465.

[52] R. Senin, A.C. Ion, O. Oprea, R. Stoica, Sorption of Bisphenol A in Aqueous Solutions on Irradiated and as-Grown Multiwalled Carbon Nanotubes, (2018). ⟨https://doi.org/10.37358/RC.18.5.6297⟩.

[53] C. Nguyen-Huy, N. Kim, T.-D. Nguyen-Phan, I.-K. Yoo, E.W. Shin, Adsorptive interaction of bisphenol A with mesoporous titanosilicate/reduced graphene oxide nanocomposite materials: FT-IR and Raman analyses, Nanoscale Res. Lett. 9 (2014) 462, https://doi.org/10.1186/1556-276X-9-462.

[54] D. Balarak, F.K. Mostafapour, S.M. Lee, C. Jeon, Adsorption of bisphenol A using dried rice husk: equilibrium, kinetic and thermodynamic studies, Appl. Chem. Eng. 30 (2019) 316–323, https://doi.org/10.14478/ace.2019.1013.

[55] G. Liu, X. Li, J.-W. Lee, B.N. Popov, A review of the development of nitrogen-modified carbon-based catalysts for oxygen reduction at USC, Catal. Sci. Technol. 1 (2011) 207–217, https://doi.org/10.1039/C0CY00053A.

[56] J. Yu, Y. Luan, Y. Qi, J. Hou, W. Dong, M. Yang, G. Wang, Hierarchical PS/PANI nanostructure supported Cu(ii) complexes: facile synthesis and study of catalytic applications in aerobic oxidation, RSC Adv. 4 (2014) 55028–55035, https://doi.org/10.1039/C4RA06944G.

[57] H.J. Kim, I.S. Bae, S.J. Cho, J.H. Boo, B.C. Lee, J. Heo, I. Chung, B. Hong, Synthesis and characteristics of NH2-functionalized polymer films to align and immobilize DNA molecules, Nanoscale Res. Lett. 7 (2012) 1–7, https://doi.org/10.1186/1556-276X-7-30.

[58] T. Xing, Y. Zheng, L.H. Li, B.C.C. Cowie, D. Gunzelmann, S.Z. Qiao, S. Huang, Y. Chen, Observation of active sites for oxygen reduction reaction on nitrogen-doped multilayer graphene, ACS Nano 8 (2014) 6856–6862, https://doi.org/10.1021/nn501506p.

[59] W. Yin, C.A. Tao, X. Zou, F. Wang, T. Qu, J. Wang, The tuning of optical properties of nanoscale MOFs-based thin film through post-modification, Nanomaterials 7 (2017) 242, https://doi.org/10.3390/nano7090242.

[60] H. Khajavi, H.A. Stil, H.P.C.E. Kuipers, J. Gascon, F. Kapteijn, Shape and transition state selective hydrogenations using egg-shell Pt-MIL-101(Cr) catalyst, ACS Catal. 3 (2013) 2617–2626, https://doi.org/10.1021/cs400681s.

[61] S. Li, Y. Yang, H. Shan, J. Zhao, Z. Wang, D. Cai, P. Qin, J. Baeyens, T. Tan, Ultrafast and ultrahigh adsorption of furfural from aqueous solution via covalent organic framework-300, Sep. Purif. Technol. 220 (2019) 283–292, https://doi.org/10.1016/j.seppur.2019.03.072.

[62] A.-N. Meng, L.-X. Chaihu, H.-H. Chen, Z.-Y. Gu, Ultrahigh adsorption and singlet-oxygen mediated degradation for efficient synergetic removal of bisphenol A by a stable zirconium-porphyrin metal-organic framework, Sci. Rep. 7 (2017) 6297, https://doi.org/10.1038/s41598-017-06194-z.

[63] F.-X. Qin, S.-Y. Jia, Y. Liu, H.-Y. Li, S.-H. Wu, Adsorptive removal of bisphenol A from aqueous solution using metal-organic frameworks, Desalin. Water Treat. 54 (2015) 93–102, https://doi.org/10.1080/19443994.2014.883331.

[64] M. Zhou, Y. Wu, J. Qiao, J. Zhang, A. McDonald, G. Li, F. Li, The removal of bisphenol A from aqueous solutions by MIL-53(Al) and mesostructured MIL-53(Al), J. Colloid Interface Sci. 405 (2013) 157–163, https://doi.org/10.1016/j.jcis.2013.05.024.

[65] H.B. Senturk, D. Ozdes, A. Gundogdu, C. Duran, M. Soylak, Removal of phenol from aqueous solutions by adsorption onto organomodified Tirebolu bentonite: equilibrium, kinetic and thermodynamic study, J. Hazard. Mater. 172 (2009) 353–362, https://doi.org/10.1016/j.jhazmat.2009.07.019.

[66] C.A. Staples, P.B. Dome, G.M. Klecka, S.T. Oblock, L.R. Harris, A review of the environmental fate, effects, and exposures of bisphenol A, Chemosphere 36 (1998) 2149–2173, https://doi.org/10.1016/s0045-6535(97)10133-3.

[67] Q. Deng, C. Chen, Q. Lei, J. Liang, T. Zhang, J. Jiang, Adsorption of aniline from aqueous solution using graphene oxide-modified attapulgite composites, RSC Adv. 8 (2018) 23382–23389, https://doi.org/10.1039/C8RA04143A.

[68] M. Cuevas, S.M. Quero, G. Hodaifa, A.J.M. López, S. Sánchez, Furfural removal from liquid effluents by adsorption onto commercial activated carbon in a batch heterogeneous reactor, Ecol. Eng. 68 (2014) 241–250, https://doi.org/10.1016/j.ecoleng.2014.03.017.

[69] K.J. Zeitsch, 13. Treatment of furfural waste water, in: The Chemistry and Technology of Furfural Its Many By-Products, Elsevier, 2000, pp. 92–97.

[70] L. Pu, Y. Sun, Z. Zhang, Hydrogen bonding of hydrates of double acetic acid molecules, J. Phys. Chem. A 113 (2009) 6841–6848, https://doi.org/10.1021/jp902634h.

[71] L. Cui, J. Wei, X. Du, X. Zhou, Preparation and evaluation of self-assembled porous microspheres–fibers for removal of bisphenol a from aqueous solution, Ind. Eng. Chem. Res. 55 (2016) 1566–1574, https://doi.org/10.1021/acs.iecr.5b04306.

[72] W. Libbrecht, K. Vandaele, K. De Buysser, A. Verberckmoes, J.W. Thybaut, H. Poelman, J. De Clercq, P. Van Der Voort, Tuning the pore geometry of ordered mesoporous carbons for enhanced adsorption of bisphenol-A, Materials 8 (2015) 1652–1665, https://doi.org/10.3390/ma8041652.

[73] B.N. Bhadra, J.K. Lee, C.-W. Cho, S.H. Jhung, Remarkably efficient adsorbent for the removal of bisphenol A from water: bio-MOF-1-derived porous carbon (https://doi.org/), Chem. Eng. J. 343 (2018) 225–234, https://doi.org/10.1016/j.cej.2018.03.004.

[74] S. Bele, V. Samanidou, E. Deliyanni, Effect of the reduction degree of graphene oxide on the adsorption of Bisphenol A, Chem. Eng. Res. Des. 109 (2016) 573–585, https://doi.org/10.1016/j.cherd.2016.03.002.
[75] S. Rovani, J.J. Santos, S.N. Guilhen, P. Corio, D.A. Fungaro, Fast, efficient and clean adsorption of bisphenol-A using renewable mesoporous silica nanoparticles from sugarcane waste ash, RSC Adv. 10 (2020) 27706–27712, https://doi.org/10.1039/D0RA05198E.
[76] Y.-H. Kim, B. Lee, K.-H. Choo, S.-J. Choi, Selective adsorption of bisphenol A by organic–inorganic hybrid mesoporous silicas, Microporous Mesoporous Mater. 138 (2011) 184–190, https://doi.org/10.1016/j.micromeso.2010.09.007.
[77] D. Bůžek, S. Ondrušová, J. Hynek, P. Kovář, K. Lang, J. Rohlíček, J. Demel, Robust aluminum and iron phosphinate metal–organic frameworks for efficient removal of Bisphenol A, Inorg. Chem. 59 (2020) 5538–5545, https://doi.org/10.1021/acs.inorgchem.0c00201.